![Argonne National Laboratory logo]

Thermochemical Property Measurements of FLiNaK and FLiBe in FY 2020

Chemical and Fuel Cycle Technologies Division

Thermochemical Property Measurements of FLiNaK and FLiBe in FY 2020

by
T. Lichtenstein, M.A. Rose, J. Krueger, E. Wu, and M.A. Williamson
Chemical and Fuel Cycle Technologies Division, Argonne National Laboratory

February 17, 2022

CONTENTS

Summary of Changes in Revision 1

The report was updated to include results of additional compositional analyses of FLiBe and heat capacity measurements for liquid FLiNaK and FLiBe. An improved method of analysis resulted in values for FLiNaK that are higher than originally reported, but they are still lower than literature values. The collection of FLiBe measurements were analyzed in aggregate and it was determined that high concentrations of dissolved oxygen, and graphite impurities in the source salt resulted in heat capacity values that are significantly lower than literature values for FLiBe. Comments relating measured values to literature values for liquid FLiBe have been deleted. The discussion in Section 5 includes a new figure showing the role of the inclusion of first-order phase transitions on the measured heat capacity. The discussion in Section 5.2 was updated to include the above information and a reference to the published values for the heat capacity of BeO. The conclusions were updated based on the above information.

1.   Introduction

The technical bases and methods developed at Argonne to measure thermochemical properties of molten salt mixtures are summarized and results provided to show the precision achieved. These methods include measurements of phase transition temperatures and heat capacity at temperatures to approximately 700 °C for eutectic mixture of 46.5-11.5-42.0 mol% LiF-NaF-KF (FLiNaK) and 67-33 mol% LiF-BeF$_2$ (FLiBe). Details of procedures, calibrations and operation of instruments are discussed, and results are compared with values available in the literature. Additional discussions address the sources of error and estimated uncertainties in the reported values.

2.   Source Materials and Salt Preparation

Reagents used to prepare salt mixtures for measurements were purchased at the highest purities available (better than 99.9% by trace metals analysis). Appendix A provides material certificates for representative salt reagents provided by the manufacturers.

Salt mixtures and samples to be analyzed were prepared in argon atmosphere gloveboxes in which oxygen and moisture levels are both maintained at below 10 ppm. Reagent salts were characterized by using powder X-ray diffraction prior to use to confirm the compositions and determine if significant amounts of impurities were present. Samples were fixed onto slides with double-sided tape and sealed with Kapton polymer film while inside the glovebox to avoid contamination throughout the analysis. A Bruker D5000 X-ray diffraction (XRD) system was used to measure the pattern over the range $2\theta = 10°$ to $100°$. Figure 1 shows the XRD diffraction patterns measured for the reagent LiF, KF, and NaF. The circles indicate the intensities and locations of peaks listed in the International Center for Diffraction Data database that were used to confirm the identities of the reagent salts.

Beryllium fluoride was purchased as industrial grade material from Materion. The salt particles had an abundance of visible dark-colored inclusions thought to be graphite; a representative grain is shown in Figure 2. Steps were taken to purify the material before producing salt mixtures for analysis. The first step of purification was to manually remove visible pieces of graphite from the material. The salt was then heated at 300 °C to remove adsorbed water. The BeF$_2$ salt was then melted and held at 700 °C to allow minute pieces of solid impurities to either settle to the bottom or rise to the top of the molten salt. After cooling to solidify, the top and bottom sections of the salt block were removed and discarded. The relatively pure middle portion was ground and the process repeated several times until there was no visible color change in the salt from top to bottom and no impurities were observed. Three samples of BeF$_2$ purified in this manner were analyzed for total dissolved oxygen using a LECO 836 Oxygen/Nitrogen Analyzer.
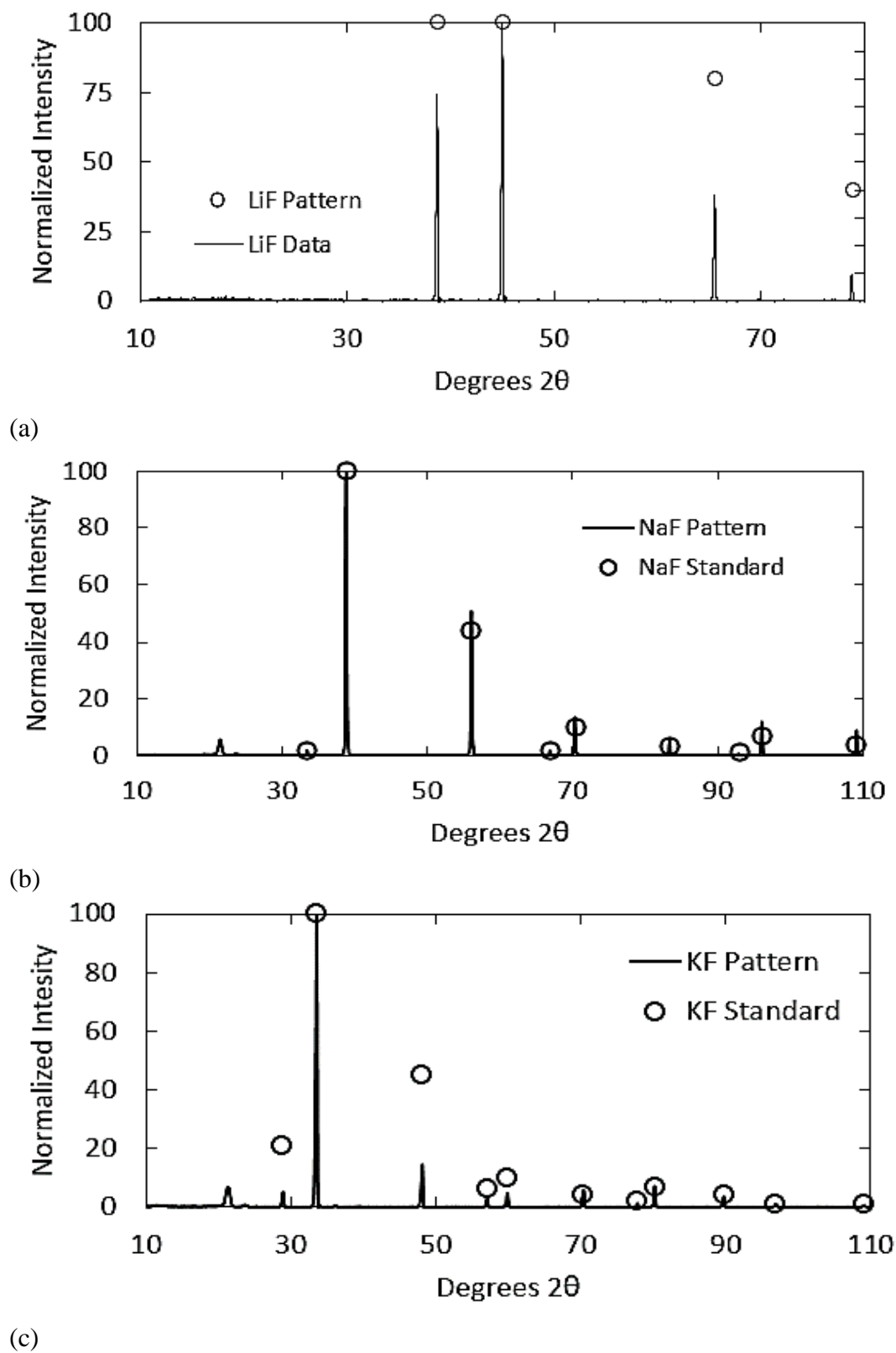
Figure 1: Measured X-ray Diffraction Patterns and Peak Intensity compared with Literature Data for Reagent Salts (a) LiF, (b) NaF, and (c) KF
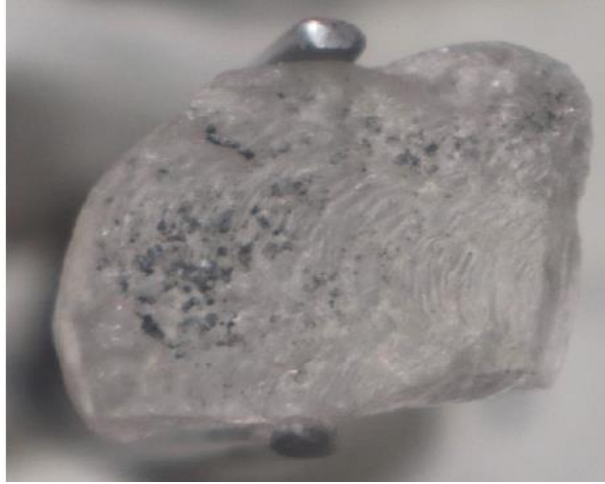
Figure 2. Photograph of As-Received BeF₂ Salt Granule

Table 1 shows the results of that analysis; the results are accurate within 25% of the reported values. The measured oxygen content includes that in oxides and water impurities.

Table 1. Results of Oxygen Analysis of BeF₂ Samples

Sample #	Oxygen (wt %)
1	1.2
2	1.3
3	1.2

Salt mixtures were prepared by placing the appropriate amounts of reagent salts in a nickel crucible and heating twice in a furnace to melt and homogenize the material. The as-batched compositions of the two mixtures are shown in Table 2. The nickel crucible was manually polished with steel wool and rinsed with methanol to remove any oxide residue and prevent oxide contamination of the mixtures. The fused salt was removed from the crucible and ground to a fine powder after each heating by using a mortar and pestle.

Table 2: As-batched Compositions of FLiNaK and FLiBe Salts

FLiNaK (g)[*]			FLiBe (g)	
LiF	NaF	KF	LiF	BeF_2
2872.15	1123.43	5773.59	524.3463	468.0840

*Based on [1].

Wet analytical methods were used to analyze the elemental compositions of salt batches used for each property measurement. Replicate samples were dissolved in nitric acid and analyzed by inductively coupled plasma-optical emission spectroscopy (ICP-OES) using a Perkin Elmer Optima Model 8300DV ICP-OES. Analyses were performed to determine the homogeneity of the mixture and the results are collected in Table 3 for major elements of FLiNaK and Table 4 for FLiBe, represented as the constituent fluorides. The averages and one standard deviation for the triplicate analyses are included.

Table 3: Major Elemental Analysis of FLiNaK by ICP-OES (mol %) [1]

	LiF	NaF	KF
Sample 1	47.0	11.6	41.4
Sample 2	46.3	11.6	42.1
Sample 3	46.1	11.3	42.6
Average	46.5	11.5	42.0
1 s	0.5	0.2	0.6

Table 4: Major Elemental Analysis of FLiBe by ICP-OES (mol %)

	LiF	BeF_2
Sample 1	67.2	32.8
Sample 2	67.2	32.8
Sample 3	67.2	32.8
Average	67.2	32.8
1 s	0.0	0.0

Aliquots of the solutions used for ICP-OES analyses were further diluted and used to measure the amounts of trace contaminants in each FLiNaK and FLiBe salt sample by using inductively coupled plasma-mass spectrometry (ICP-MS); those results are shown in Table 5 and 6 for FLiNaK and FLiBe, respectively. The ICP-MS technique is typically accurate to ±10%. The levels of Mg, Cr, Mn, Rb, and Cs measured in the salts are consistent with the contamination levels measured in the reagents. However, the concentrations of Ni and Ca measured in the FLiNaK salt were significantly higher than the concentrations measured in any of the reagents. Nickel contamination of the salt may have come from the nickel crucible used for melting the salt and the nickel impeller used to stir the molten salt. The calcium contamination was likely introduced after production when the salt was ground using a large ceramic mortar and pestle. The slightly elevated iron contamination in the FLiBe samples may have come from the steel wool used to polish the nickel crucibles.

Table 5: Trace Element Analysis of FLiNaK by ICP-MS (ppm) [1]

	Mg	Ca	Cr	Mn	Fe	Ni	Rb	Cs
Sample 1	< 82	1490	< 11	< 4	< 200	115	31.9	2.3
Sample 2	< 30	944	< 8	< 2	< 140	137	25.8	1.8
Sample 3	< 25	510	< 7	< 3	< 120	118	26.3	1.4
Average		981				123	28.0	1.8
1 s		490				12	3.4	0.4

< values give detection limits.

Table 6: Trace Element Analysis of FLiBe by ICP-MS (ppm)

	Mg	Ca	Cr	Mn	Fe	Ni	Rb	Cs
Sample 1	47.4	< 286	3.33	3.97	24.8	7.3	0.34	0.69
Sample 2	68.9	< 577	3.35	5.03	53.5	10.1	0.38	0.46
Sample 3	48.7	< 255	4.89	4.30	35.6	7.1	0.38	0.18
Average	55.0		3.90	4.40	38.0	8.2	0.40	0.44
1 s	9.9		0.73	0.44	11.9	1.4	0.02	0.21

< values give detection limits.

3.   Thermal Analysis by Differential Scanning Calorimetry

Differential scanning calorimetry (DSC) is used to perform thermal analysis of salt systems and measure the heat capacity. Hermetically sealed gold sample crucibles (TA Instruments, Wood Dale, IL) are used to contain salts for analysis, as pictured in Figure 3. The gold cells are cleaned before use by washing first with water, then with concentrated hydrochloric acid, and then again
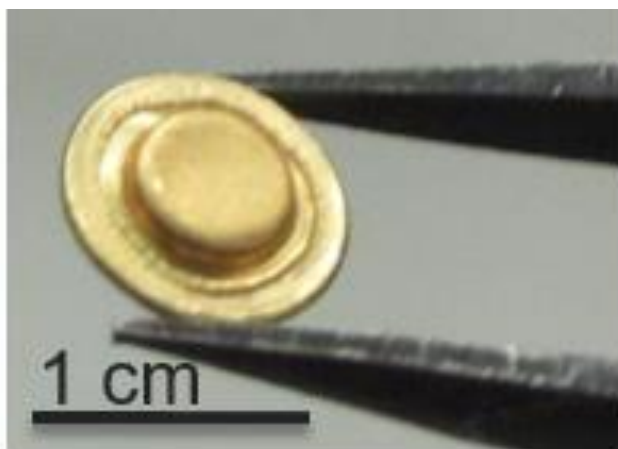

Figure 3: Hermetically Sealed Gold Sample Crucible Showing Sealed Side

with water. The cells are allowed to air dry before being placed in the air lock of the glovebox, which is then evacuated using a mechanical pump for 30-60 minutes before the cells are moved into the glovebox. The gold cells are carefully weighed then loaded with crushed salt and sealed twice by using a mechanical sealer. This procedure ensures that the salt samples are not exposed to an atmosphere with greater than 10 ppm oxygen and 1 ppm water, which are the upper limit values maintained in the glovebox, either prior to or during DSC analyses.

Thermal properties of the salt samples are measured by using a Netzsch (Model STA Jupiter 449C) standard thermal analyzer (STA) with thermogravimetric analysis (TGA). The STA is operated inside of an argon atmosphere glovebox maintained at less than 10 ppm oxygen and less than 1 ppm water. A continuous high purity argon purge inside of the instrument is used to provide an atmosphere surrounding the sample with even lower oxygen and moisture conditions during measurements. Prior to the heat capacity measurements, each sealed crucible containing a salt sample is heated to a temperature above the melting point of the sample to ensure the material is well mixed and the crucible is well sealed. The sample is subsequently heated twice at 5 °C min^{-1} using the heating profile shown in Figure 4 to measure the melting point and detect other phase transitions. Two sequential analyses are run to verify system stability.
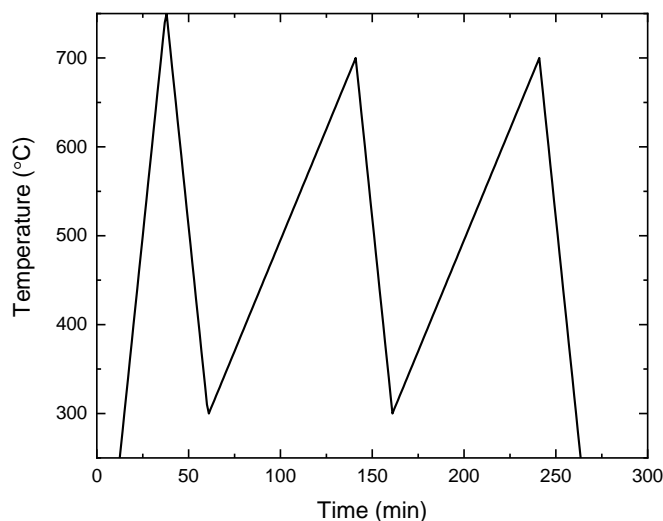
Figure 4. Heating Profile to Determine Phase Transition Reactions.

3.1   Temperature Calibration of DSC

The temperatures measured by the DSC are calibrated before use by measuring the melting points of five pure metal standards from Netzsch (Sn, Zn, Al, Ag, and Au) having known values that span the range from 231.9 to 1064.2 °C. The melting point of each metal standard is measured twice at the same heating rate of 5 °C min^{-1} used to analyze the salt samples and by the same method. A

representative thermogram measured for a Zn standard is shown in Figure 5. The melting point is determined from the onset temperature, labelled T_{onset}, which is the temperature at which the extrapolated baseline meets the linear extrapolation from the inflection point of the heating curve (illustrated by the dashed lines in Figure 5). This is done automatically by the software used to run the scan.
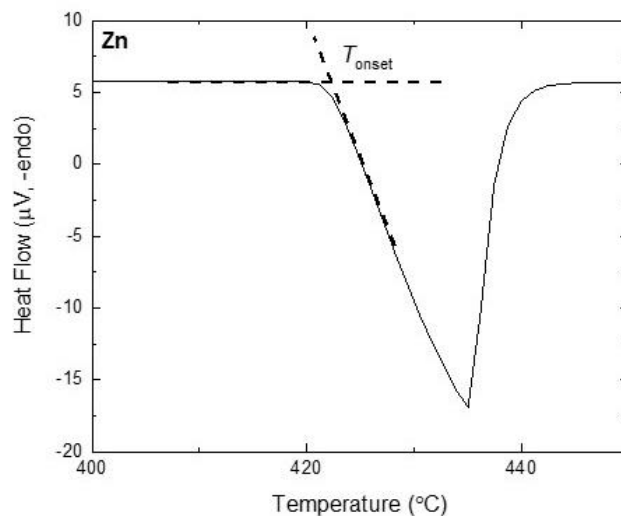
Figure 5. Determination of the Transition Temperature by Onset Extrapolation for Pure Zn.

The repeatability is typically excellent for duplicate measurements made with each metal standard, but the measured melting temperatures usually differ slightly from the reference values used by the software due to uncontrollable variables. Figure 6 shows the results of duplicate calibration measurements made prior to salt measurements expressed as Delta T = T(measured)-T(reported).
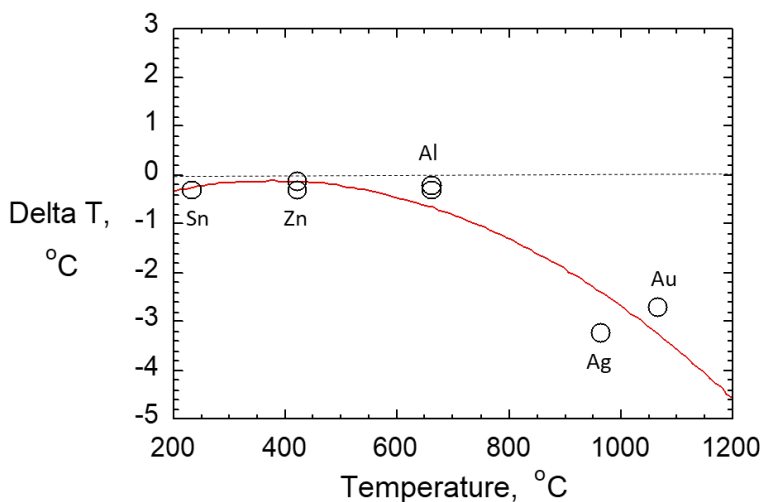
Figure 6: Calibration curve for duplicate measurements of metal standards prior to DSC analyses of salts

Duplicate measurements for Sn, Ag, and Au overlap but small differences are seen for Zn and Al. A quadratic regression is used by the Netzsch Proteus software to calibrate the measured temperatures over the full range using the reported values for the metal standards. The difference between the values of the calibration curve at the melting temperature of each standard metal and the measured value represents the accuracy of measurements made at and near that temperature.

All calibration results are being tracked to detect significant changes in performance and long-term bias of the DSC. A summary of the mean calibration metal melting temperatures are shown in Table 7 along with values for two standard deviations (2s), which quantify the precision of measurements at each temperature. Calibrations made at different times resulted in slightly different calibrations curves due to environmental effects, but the accuracies were always within about 1 °C for temperatures below 700 °C and 2 °C for temperatures above 700 °C. These differences are taken into account by using the calibration curve. No bias has been observed through about 2.5 years of operation and the deviations between reported and measured melting temperature remain within 2 °C for temperatures up to 660 °C and within about 4 °C at higher temperatures.

Table 7: Mean Melting Temperatures for Calibration Metals Measured by DSC over 2.5 Years

Calibration Metal	Sn	Zn	Al	Ag	Au
Reported Melting T, °C	231.9	419.6	660.3	961.8	1064.2
Mean Measured Melting T, °C	231.0	419.8	660.8	959.3	1062.4
2 s, °C	0.8	2.0	0.9	2.2	3.8

3.2　Thermal Analysis of FLiNaK Salt

Three portions of the FLiNaK salt (21.11 mg, 24.57 mg, and 24.64 mg) were hermetically sealed in gold cells under an inert atmosphere for thermal analysis. Figure 7 shows the signals from the heating cycles of duplicate DSC scans of each sample run at 5 °C min^{-1} on the same plot, with solid and dashed lines representing the first and second runs, respectively. The repeatability observed in the replicate scans indicates the system remained stable during the analyses. The small differences in the shapes of the scans of the three samples are due to minor differences in the environment on the days the scans were made. No peaks other than the eutectic melting peak are seen, although a small shoulder is noticeable at approximately 465 °C in some scans.

The Netzsch software Proteus was used to determine the onset temperature of the eutectic peak in each scan and the results are listed in Table 8. The average of the measured melting onset temperatures was 456.2 °C and the standard deviation was 0.6 °C. The instrument was calibrated prior to use and the precision of DSC measurements has been determined to be ±1 °C up to 700 °C
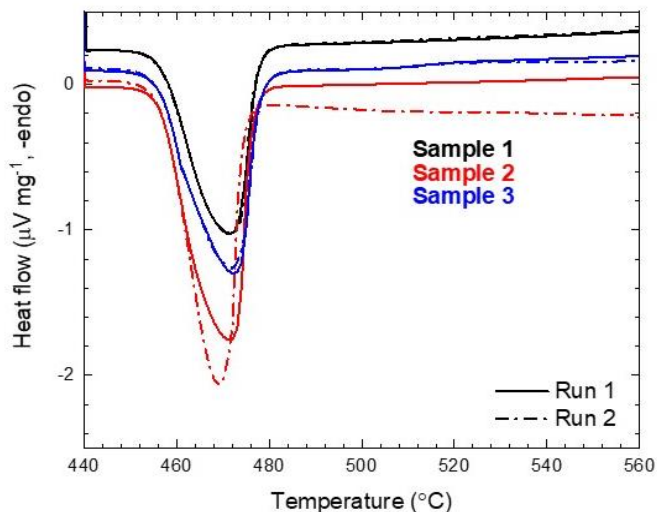
Figure 7: DSC Scans of FLiNaK Salt Samples at 5 °C min^{-1} Scan Rate

Table 8: Measured Onset Temperatures for Eutectic FLiNaK

Sample	Run	Onset Temperature (°C)
1	1	455.8
	2	456.1
2	1	456.5
	2	456.9
3	1	456.5
	2	455.2
Average		456.2
1 s		0.6

based on replicate calibrations with five different metallic standards. The same method was used to determine the onset melting temperatures of the standards during calibration runs and analyses of the salt samples. The variations in the measured onset melting temperatures of the three samples listed in Table 8 are within the instrumental uncertainty.

To verify the stability of liquid FLiNaK heat flows, a sample was subjected to 11 cycles of heating-cooling through the melting temperature, shown in Figure 8. The heat flow of the liquid was unchanged and the onset of the eutectic was stable across cycles to within 0.3 °C, which is well within the accuracy of the calibration and indicates that the composition of the FLiNaK sample and thermal contact with the crucible remained stable.
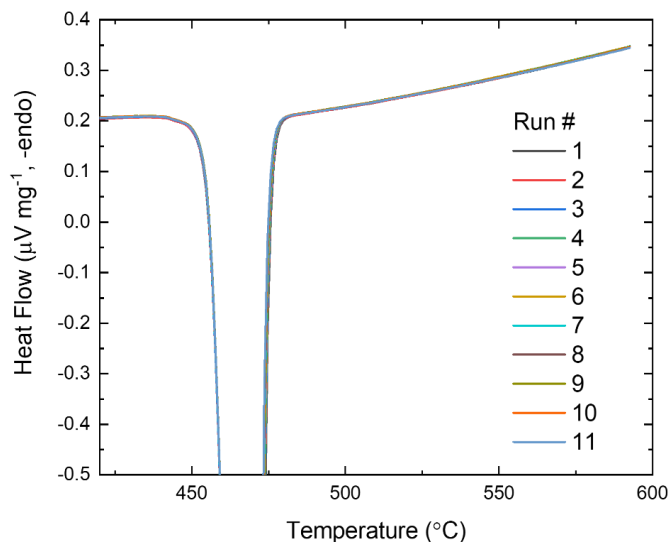
Figure 8: Eleven Consecutive Heating-Cooling Cycles on a FLiNaK Sample

3.3 Thermal Analysis of FLiBe Salt

Three portions of the FLiBe salt (21.82 mg, 21.83 mg, and 21.73 mg) were prepared for thermal analysis in the same manner as described for FLiNaK in Section 3.2. Figure 9 shows the signals from the heating cycles of duplicate DSC scans with each sample run at 5 °C min^{-1} on the same plot. The repeatability of the replicate scans indicates the FLiBe salt remained stable during the analyses. The small differences in the shapes of the DSC scans with the three samples are due to minor differences in the environment on the three days the scans were made. Two peaks are seen in each scan. The smaller peak at ~416 °C labelled Reaction 1 in Figure 9 corresponds to the eutectic transition reaction where the two-phase solid of BeF_2 and Li_2BeF_4 melts. The larger peak that occurs at ~452 °C and is labelled Reaction 2 corresponds to the congruent melting of Li_2BeF_4. The transition temperatures measured in the thermal analyses are collected in Table 9.

Table 9: Measured Transition Temperatures for FLiBe

Sample	Run	Transition Temperature (°C)	
		Reaction 1	Reaction 2
1	1	418.6	453.2
	2	416.9	452.5
2	1	416.6	452.3
	2	413.9	450.2
3	1	417.6	452.4
	2	415.9	452.0
Average		416.6	452.1
1 s		1.5	0.9
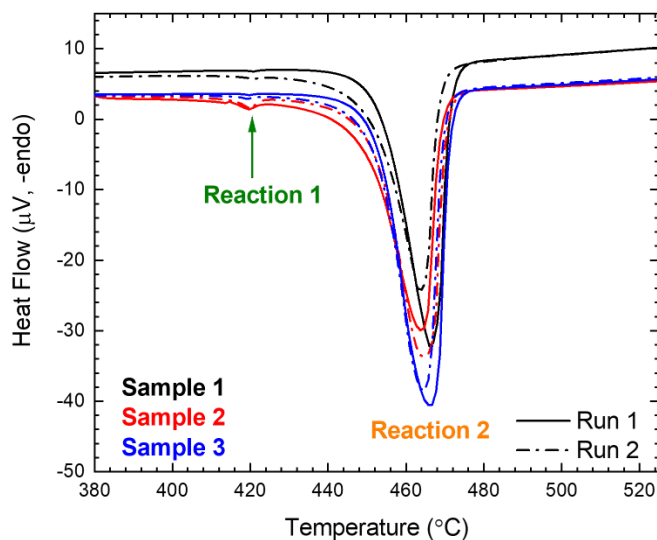
Figure 9: DSC Scans of FLiBe Salt Samples

The high temperature Reaction 2 is measured to occur close to the literature value of 459 °C [2] but the low temperature Reaction 1 occurs about 53 °C higher than the literature value of 363 °C [3]. The thermal analysis reported in literature was based on heating and cooling curves at 1–2 °C min^{-1} but the scan rate used to identify the eutectic at 363 °C was not indicated, so undercooling during the cooling scan may have resulted in the reported value being too low.

A scan was performed over an expanded temperature range to verify no additional reactions occurred in our analyses and both the heating and cooling curves are shown in Figure 10. The heating curve has no features at temperatures below 380 °C, which suggests that the feature
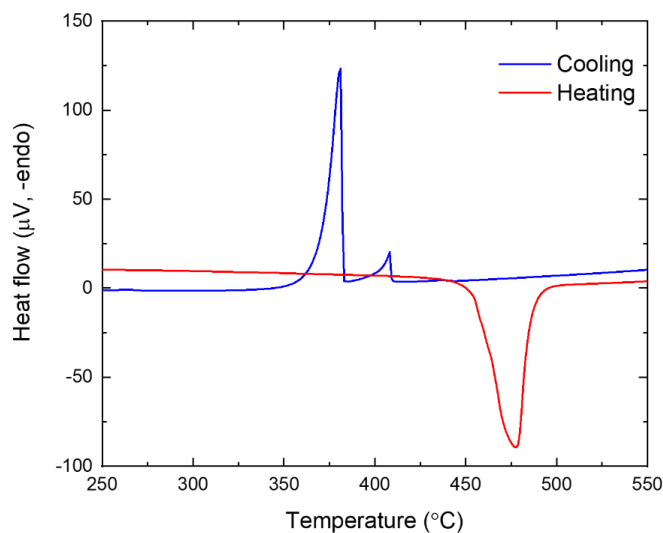
Figure 10: Expanded Temperature Range Heating-Cooling DSC Scan for FLiBe

observed at 416°C is most likely due to the eutectic transition reaction. This is confirmed by the two peaks seen in the cooling curve that reflect the reverse of the two transition reactions observed in the heating curve. Undercooling of 30–50 °C is also observed in the comparison, with the small peak occurring at 408 °C signaling the start of solidification and the large peak occurring at 381 °C being associated with the completion of solidification. This result indicates the value of 363 °C reported in the literature [3] is probably affected by supercooling and the value of 416.6 °C is more accurate.

4.   Heat Capacity Measurements

4.1   Heat Capacity Measurement Method

The heat capacity measurements follow a standard three-step procedure adapted from that described in ASTM E1269 [4]. This includes separate measurements with two empty crucibles, with a sapphire reference and an empty crucible, and with a salt sample and an empty crucible. The procedure employed at Argonne uses gold crucibles that are weight-matched to within 1.5% for all measurements. The sapphire reference and salt samples sealed within the gold crucibles are weight matched to within 1%. The three measurements are made following the thermal profile illustrated in Figure 11 for salt measurements: a 15-minute isothermal hold to measure the heat flow at 470 °C, a linear ramp at 10 °C min^{-1} to 730 °C, then a 15-minute isothermal hold to measure the heat flow at 730 °C.

Figure 11. Heating Profile for Heat Capacity Measurements.

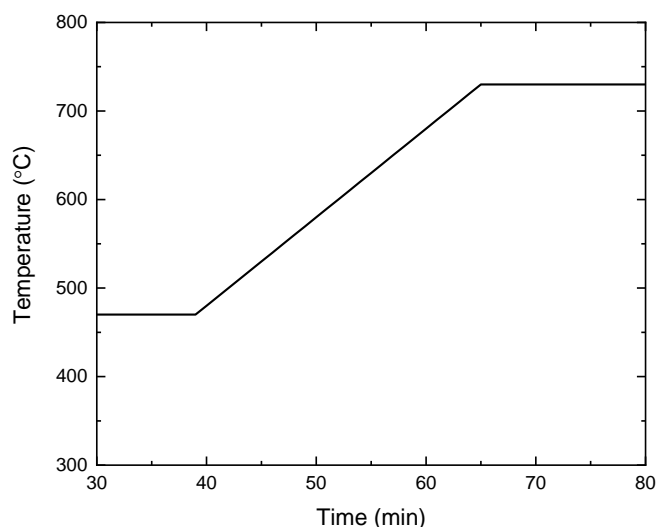An instrumental baseline using two empty, weight-matched crucibles is run first to determine the instrument bias. One of the empty crucibles is replaced with a crucible containing a sapphire standard and run in the same thermal profile, then the sapphire crucible is replaced with a crucible containing a salt sample and run using the same thermal profile. Heat flows through the sapphire and salt sample are corrected for the instrumental bias by subtracting the heat flow of the instrument baseline determined in the first step with empty crucibles. The baseline correction is done automatically by the Netzsch Proteus software.

In the Argonne procedure, the heat flows measured at each temperature are also corrected for environmental stability-related effects by using differences in the heat flows measured during isothermal holds before and after the linear ramp. A linear baseline is interpolated between those measured values to represent temperature-dependent environmental stability effects. Values of the interpolated baseline are calculated as a function of time during the temperature ramp by using Equation 1.

$$\varphi_{iso}(t) = \varphi_{iso,st} + \frac{\varphi_{iso,end} - \varphi_{iso,st}}{t_{end} - t_{st}} (t - t_{st}) \tag{1}$$

where $\varphi_{iso,st}$ is the heat flow measured at the end of the low temperature hold, $\varphi_{iso,end}$ is the heat flow measured at the end of the high temperature hold, t_{st} is the time at the start of the heating ramp, and t_{end} is the time at the end of the ramp. The corrected heat flow, $\varphi_{corr}(t)$, at each point during the ramp is calculated by subtracting the interpolated baseline, $\varphi_{iso}(t)$, from the experimental heat flow, $\varphi_{exp}(t)$, as indicated in Equation 2. The method is visualized in Figure 12.

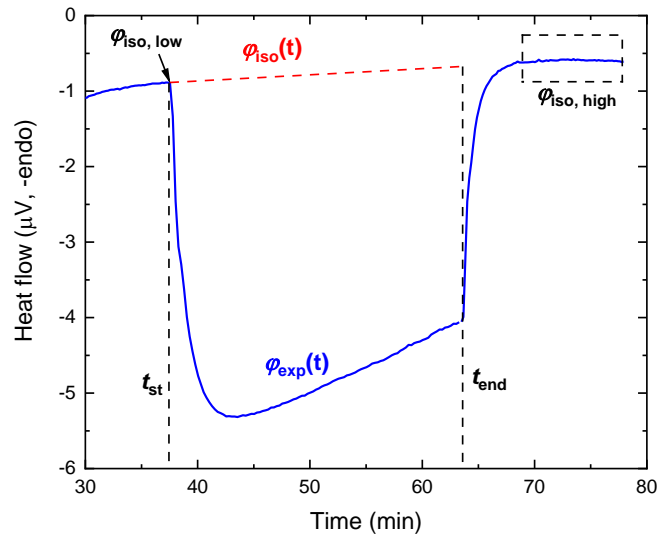$$\varphi_{corr}(t) = \varphi_{exp}(t) - \varphi_{iso}(t) \tag{2}$$

Figure 12. Visual Representation of the Correction of Heat Flow using Isotherms

Differences in the heat flows measured during isotherms at 470 °C and at 730 °C can be caused by material properties, thermal contacts, and changes in environmental conditions during the DSC measurement. Data from experiments where the DSC signals of the two isothermal holds differ by more than 2 µV are considered to indicate system instability and the results are discarded.

The heat capacity of the sample, C_p^s, is calculated relative to the heat flows measured for the sample and reference material scaled by the material and crucible masses by:

$$C_p^s = \frac{m_r}{m_s} \frac{\Delta\varphi_{corr,s}}{\Delta\varphi_{corr,r}} C_p^r + \frac{m_{cr}^r - m_{cr}^s}{m_s} C_p^{cr} \tag{3}$$

where m_s and m_r are the masses of the sample and sapphire; m_{cr}^s and m_{cr}^r are the masses of the crucibles containing the sample and sapphire; $\Delta\varphi_{corr,s}$ and $\Delta\varphi_{corr,r}$ are the heat flows of the sample and sapphire, both corrected for the baseline and isothermal drifts; and C_p^s, C_p^r, and C_p^{cr} are the heat capacities of the sample, sapphire, and crucible, respectively.

4.2   Heat Capacity of FLiNaK Salt

Three samples of the FLiNaK salt (referred to as S1, S2, and S3) were prepared for heat capacity measurements. The sample and sapphire masses for the three measurements are given in Table 10.

Table 10: Samples and Sapphire Used for FLiNaK Heat Capacity Measurements

	Sapphire A	S1	Sapphire B	S2	S3
Sample mass (mg)	21.82	21.88	21.46	21.54	21.57
Crucible mass (mg)	372.39	371.38	382.42	387.0	379.40

The measurements were run and signals corrected using the procedure described in Section 4.1. The corrected DSC signals were used to calculate the heat capacity of FLiNaK salt by using Equation 3. Figure 13 shows the calculated heat capacity values for FLiNaK samples S1, S2 and S3 plotted as a function of temperature in for liquid-state FLiNaK and values at selected temperatures are tabulated in Table 11.

Table 11. Calculated Heat Capacity at Select Temperatures for FLiNaK Salt

Temperature (°C)	Heat Capacity (J g^{-1} K^{-1})		
	S1	S2	S3
600	1.64	1.66	1.65
625	1.65	1.65	1.64
650	1.65	1.64	1.64
675	1.65	1.64	1.67
700	1.65	1.67	1.68
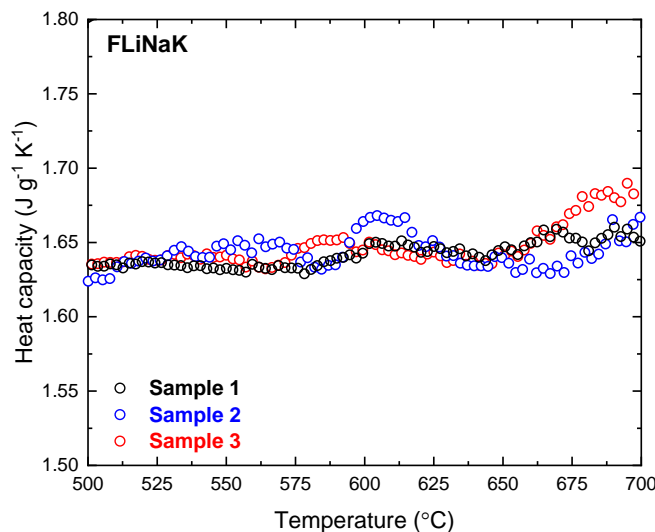
Figure 13. Calculated Heat Capacity of FLiNaK For Samples S1, S2, and S3.

The heat capacity for liquid FLiNaK follows the expected behavior of being constant or increasing with temperature over the temperature range of 500–700 °C. The average of the measured heat capacity of FLiNaK is about 1.65 J g^{-1} K^{-1} over the temperature range of 500–700 °C with a maximum difference of 1% of the mean value for three measurements. Baseline and isothermal corrected data for heat capacity measurements of FLiNaK are shown in Figure 14. The smooth transition from the increasingly negative values at low temperatures to linearly increasing heat flow confirms the lack of phase transition for sapphire and FLiNaK 500 and 700 °C.
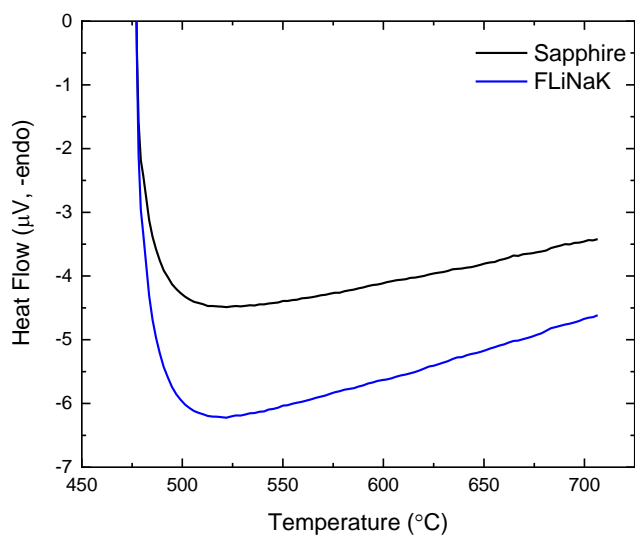
Figure 14. Baseline and Isothermal-Corrected Signals for DSC with Sapphire and FLiNaK.

4.3   Heat Capacity of FLiBe Salt

The heat capacity of FLiBe was measured using the same samples that had been used for thermal analysis. The sample and crucible masses are given in Table 12**.** The measurements for heat capacity were made as described in Section 4.1. The calculated heat capacity for FLiBe is shown graphically in Figure 15 and values at several temperatures are given in Table 13.

Table 12: Samples and Sapphire Used for FLiBe Heat Capacity Measurements

Sample	Sapphire	FLiBe		
		S1	S2	S3
Samples mass (mg)	21.82	21.82	21.83	21.73
Crucible mass (mg)	372.39	368.26	369.33	368.75
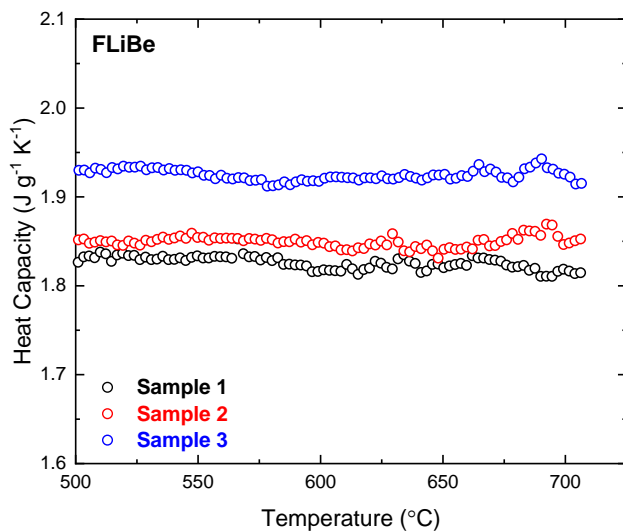
Figure 15. Calculated Heat Capacity for FLiBe Samples 1 2, and 3 (S1, S2, S3).

Table 13. Calculated Heat Capacity at Select Temperatures for FLiBe Salt

Temperature (°C)	Heat Capacity ($J\ g^{-1}\ K^{-1}$)		
	S1	S2	S3
600	1.82	1.85	1.92
625	1.83	1.85	1.92
650	1.82	1.84	1.93
675	1.82	1.85	1.92
700	1.82	1.85	1.93

Baseline and isothermal corrected data for heat capacity measurements of FLiBe are shown in Figure 16. These data confirm that no phase transitions occurred during the tested temperature range.
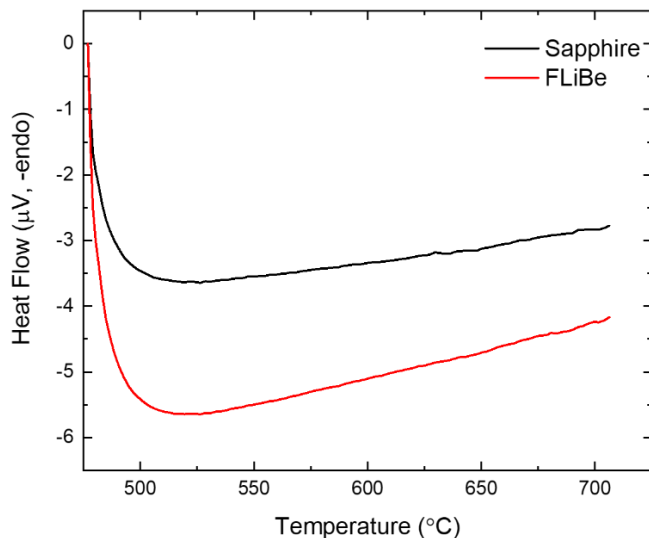

Figure 16. Baseline and Isothermal-Corrected DSC Signals for Sapphire and FLiBe

The calculated heat capacity of FLiBe and FLiNaK have similar correlations with temperature. However, there is more scatter in the calculated heat capacity of the FLiBe samples at temperatures above 600 °C than at lower temperatures. The calculated heat capacity is about 1.86 ± 0.04 J g^{-1} K^{-1} and constant between 500 and 700 °C with a maximum difference of 5% of the mean value. The precision of our FLiBe heat capacity measurements is consistent with expected precision of heat capacity measurements by DSC [5].

5. Discussion

These measurements have been repeatable with a deviation of 5% of the average values reported for FLiBe and 1% for FLiNaK. These deviations are consistent with the uncertainty expected for heat capacity measurements by DSC [5]. Major factors affecting the precision include weight matching the samples and crucibles to the sapphire standard, placement of the samples within the DSC sample carrier for all three steps, and the experimental temperature range. Differences in the weight matching of the samples and crucibles affects the heat capacity calculated using Equation 3. Sample placement in the DSC carrier across the three runs will change the $\Delta\varphi$ term and is taken into account by using differences in the measured isothermal hold values. It has been observed that improper sample placement will lead to large differences in the heat flows of the isothermal holds; proper sample placement minimizes these differences.

The calculated heat capacity from isothermal holds that differ >2 µV has been shown to differ by up to 0.5 J g^{-1} K^{-1} from values measured using the procedure described in this report. This is illustrated in Figure 17, which shows the results of FLiNaK heat capacity measurements performed using the same sample (S1) and sapphire reference on two separate days. In the measurement made on September 8th, the sapphire isothermal holds at 420 and 730 °C differed by 3.7 µV and the calculated heat capacity (Figure 17b) was ~2.03 J g^{-1} K^{-1}. The measurement made on September 10th using the same sapphire reference had a difference of 0.8 µV and the calculated heat capacity was ~1.51 J g^{-1} K^{-1}. The greater instability of the instrument during the measurement made on September 8th is manifested as excessive variance in the background that affected the calculated heat capacity. We have found greater reproducibility when isothermal holds differ by < 2 µV and both samples differ in the same manner (i.e., both become more endothermic).

(a)   (b)
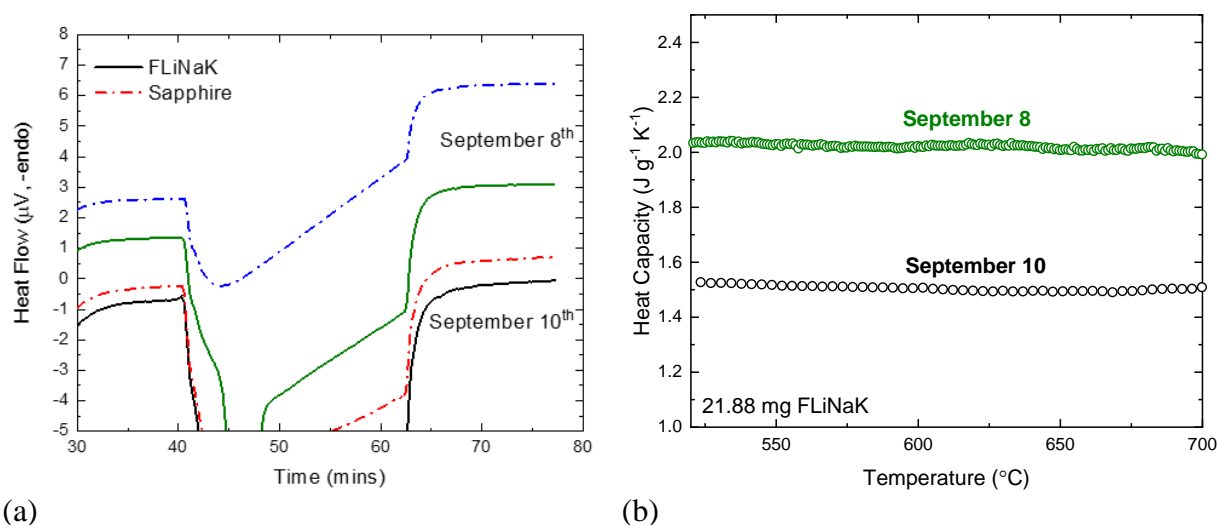
Figure 17. (a) Heat Flows for Sapphire and FLiNaK (S1) Measured on September 8th and September 10th and (b) Calculated Heat Capacity From Measurements on September 8th and September 10th.

The occurrence of a first-order phase transition (e.g., eutectic melting) within the range of linear temperature ramp has been observed to impart an artificial temperature dependence. Figure 18 shows three FLiNaK measurements, one with the inclusion of the first order phase transition during the linear temperature ramp (420 °C–730 °C temperature range) and two with low temperature isothermal holds at temperatures above the eutectic melting (470 °C–730 °C temperature range). The measured heat capacity for the measurement range including the first order phase transition has a negative temperature dependence from 525 °C–625 °C and then has minimal temperature dependence up to 700° C. In comparison, the two samples that do not include the first order phase transition during the linear temperature ramp achieve stable heat capacity values with no temperature dependence. It is likely that the lower value measured was due to the inclusion of the first-order phase transition biasing the calculated heat capacity value lower.

Figure 18. Calculated Heat Capacity Values For Measurements Including and Excluding a First-Order Phase Transition

Finally, experimental temperature ranges of only 100–200 °C have been recommended to minimize changes in instrumental bias during the time required to make the three measurements using appropriate scan rates [5]. The temperature range of interest is greater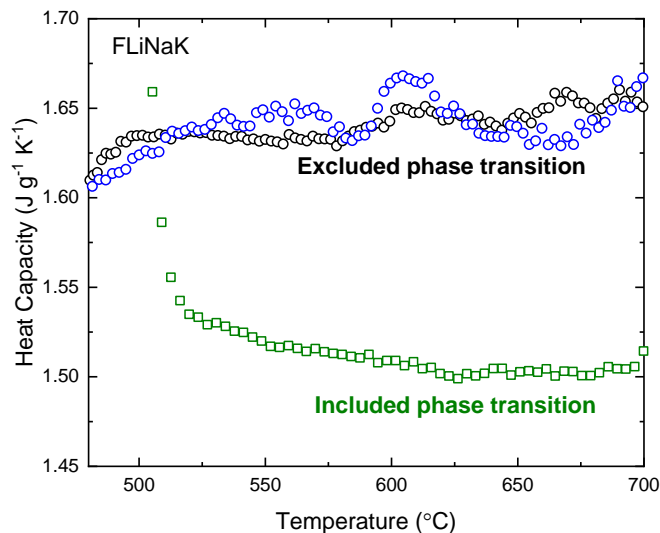 than that and the additional correction included using the heat flows measured in isothermal holds at the low and high ends of the range increases the reliability of the measured values.

5.1. Heat Capacity of FLiNaK

Examination of the available literature for the measured salts indicates the method for heat capacity measurements developed at Argonne has reduced the uncertainty of measured heat capacities compared to results in the literature. The heat capacity of FLiNaK has been reported for measurements made by drop calorimetry and by DSC. The results of drop calorimetry performed at ORNL using an ice calorimeter exhibited unquantified but significant scatter leading the researchers to conclude that only a linear fit of the measured enthalpy data with respect to temperature was justified, meaning the liquid-state heat capacity value was constant with temperature. They calculated the heat capacity of eutectic liquid FLiNaK to be 1.88 J g^{-1} K^{-1}, which was within 10% of other reported values using drop calorimetry across a multi-lab study [6].

DSC measurements with eutectic FLiNaK were performed by two groups utilizing different procedures. Rogers, Yoko, and Janz calibrated their DSC against the heats of fusion of five pure materials (In, Sn, Pb, KNO_3, LiCl-KCl) measured by drop calorimetry [7]. Calibrating the heat flow of the DSC by using heat of fusion is not recommended because the calibration is not guaranteed to be independent of temperature, the heating rate, and the crucible material [8]. Rogers, Yoko and Janz utilized hermetically sealed gold DSC cells [9] to contain a small quantity of stoichiometric eutectic FLiNaK. The sample was conditioned by 14 consecutive heating-cooling

cycles to ensure homogeneity then heated at 10 °C min^{-1} through the melting temperature. The heat capacity was calculated directly from the baseline-corrected heat flows of the sample. They determined the heat capacity of FLiNaK to range between 1.77–1.89 J g^{-1} K^{-1} at 477–587 °C with a reported repeatability within 2% [7]. Their work does not mention if isothermal measurements were used to check for deviations in heat flow and they do not mention the frequency of re-calibration of their heat flow.

The second lab using DSC, Khokhlov et al., used the same three-step procedure described in this report. They prepared FLiNaK in a similar manner described in this report but used Pt-Rh crucibles with perforated Pt-Rh lids. They performed 14 scans to precondition the FLiNaK the same as Rogers, Yoko, and Janz prior to heat capacity measurement. The heat flow of their liquid FLiNaK increased with each heating-cooling cycle from about 0.4 to 1 mW mg^{-1} for the first four reported cycles, additional increases in heat flow were not shown or mentioned in their work. Their calculated heat capacity was 1.69–1.84 J g^{-1} K^{-1} at 477–587 °C with a reported variance of 5% [10]. They did not mention if their low and high isothermal holds differed and how that would affect their data. The FLiNaK results from Rogers et al. [7] and Khokhlov et al. [10] are shown in Figure 19 overlaid with results for FLiNaK sample S1 that have been adjusted for the isothermal background by using Equation 2 (corrected) and the same results that have not been adjusted (uncorrected) and include the melting transition during the linear temperature ramps.
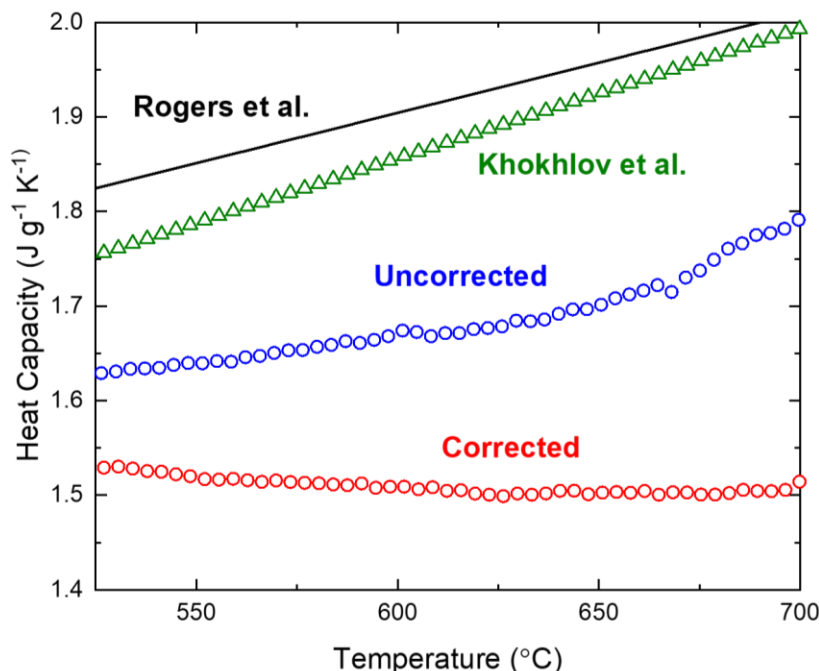

Figure 19. Overlay of the Heat Capacity of FLiNaK measured by Rogers et al., Khokhlov et al., an Uncorrected and Corrected Heat Capacity for FLiNaK sample S1 in a Scan Including the Melting Transition.

The heat capacities determined by Rogers et al. [7] and Khokhlov et al. [10] are significantly higher than our measured values that include (Figure 19) and do not include (Figure 18) the melting transition and increase with temperature. The results of Khokhlov et al. may be too high due to the increased heat flow they observed with repeated thermal cycling. Their use of perforated lids may have resulted in the loss of volatilized FLiNaK resulting in changes in the composition and unstable heat flows. Referring to Figure 8, the heat flow in our work remained stable during 11 heating-cooling cycles that confirms sample integrity was maintained by using hermetically sealed crucibles. It is important to note that the heat capacity measurements in our work and those by Khokhlov et al. were made relative to a sapphire standard and both are lower than those of Rogers et al. that determined by direct measurement without a sapphire reference. The higher values of Rogers et al. may be due to changes in conditions of their DSC after heat flow calibration. Note that our uncorrected heat capacity measurements with FLiNaK are larger in magnitude and show the same upward trend as the results of both Rogers et al. and Khokhlov et al., but the temperature dependence is removed and the magnitude lowered when results are corrected for the effect of temperature on the measured heat flow as quantified by using the isothermal holds.

5.2. Heat Capacity of FLiBe

The heat capacity of FLiBe has been calculated from drop calorimetry measurements using an ice calorimeter to be 2.32 J g^{-1} K^{-1} over the range 470–627 °C with reported uncertainties in the measurement larger than ± 3% [11]. More recent estimations of the heat capacity for FLiBe are 2.4 J g^{-1} K^{-1} with a reported accuracy of ± 20%, that is, between 1.89 and 2.84 J g^{-1} K^{-1} [12]. Our measured heat capacity of liquid FLiBe of 1.86 J g^{-1} K^{-1} is below the range reported in the literature [11]. It is likely that oxygen and graphite impurities present in our source material (approximately 1.2 wt % oxygen) lowered the heat capacity of the mixture relative to that of pure FLiBe. For example, the heat capacity of pure BeO is 1.86–1.95 J g^{-1} K^{-1} in the temperature range 527–677 °C [13] and the heat capacity of graphite is 1.55–1.73 J g^{-1} K^{-1} in the temperature range 427–627 °C [14]. In addition, the limited DSC sample size is too small to provide a representative volume for salt with impurities below a threshold concentration, and variations in impurity contents likely contributed to the imprecision of replicate measurements made with FLiBe.

6. Conclusions

Progress in improving the precision of the heat capacity measurements for molten FLiNaK and FLiBe using a DSC has been demonstrated. The method described in this report is an adaptation of the ASTM standard to molten salt systems that improves the repeatability and precision of heat capacity measurements by DSC. The improved quantification of instrumental sensitivity to the temperature scan and environmental conditions achieved by using isothermal holds enables effects of salt composition and impurities on measured values to be distinguished from measurement artifacts and imprecision. For example, the precision of heat capacity measurements made with replicate samples of relatively pure FLiNaK was very high, but variance in the impurity contents in replicate samples of contaminated FLiBe resulted in significantly lower precision. This

procedure can be directly applied to any molten salt and implemented for quality and safety basis calculations.

Acknowledgements

References

[1]. M.A. Rose, E. Wu, T. Lichtenstein, and J. Krueger "Analytical Results for FLiNaK" Argonne National Laboratory, September 2020.

[2]. J.P.M. van der Meer, R.J.M. Konings, M.H.G. Jacobs, and H.A.J. Oonk "A Miscibility Gap in LiF-BeF$_2$ and LiF-BeF$_2$-ThF$_4$." *J. Nucl. Mats.*, 344, 2005, 94–99.

[3]. R.E. Thoma, H. Insley, H.A. Friedman, and G.M. Hebert. "Equilibrium Phase Diagram of the Lithium Fluoride-Beryllium Fluoride-Zirconium Fluoride System" *J. Nucl. Mats.* 27, 1968, 166–180.

[4]. ASTM E1269 "Specific Heat Capacity by Differential Scanning Calorimeter", Annual Book of ASTM Standards, Vol. 14.02. 2005.

[5]. G.W. Hohne, W.F. Hemminger and H.-J. Flammersheim. Differential Scanning Calorimetry. Second Edition. *Springer* 2003.

[6]. W.D. Powers and G.C. Blalock "Enthalpies and Heat Capacities of Solid and Molten Fluoride Mixtures" ORNL-1956, January 1956.

[7]. D.J. Rogers, T. Yoko, and G.J. Janz. "Fusion Properties and Heat Capacities of the Eutectic LiF-NaF-KF Melt" *J. Chem. Eng. Data.* 27, 1982, 366–367.

[8]. G. Della Gatta, M.J. Richardson, S.M. Sarge, and S. Stølen. "Standard, Calibration, and Guidelines in Microcalorimetry Part 2. Calibration Standards for Differential Scanning" *Pure and Appl. Chem.* 78, 7, 2006, 1455–1476.

[9]. G.J. Janz and G.N. Truong. "Melting and Premelting Properties of the KNO$_3$-NaNO$_2$-NaNO$_3$ Eutectic System" *J. Chem. Eng. Data.* 28, 1983, 201–202.

[10]. V. Khokhlov, I. Korzun, V. Dokutovich, E. Filatov. "Heat Capacity and Thermal Conductivity of Molten Ternary Lithium, Sodium, Potassium, and Zirconium Fluorides Mixtures." *J. Nucl. Maters.* 410, 2011, 32–38.

[11]. T.B. Douglas and W.H. Payne. "Measured Enthalpy and Derived Thermodynamic Properties of Solid and Liquid Lithium Tetrafluoroberyllate, Li$_2$BeF$_4$, from 273 to 900 K" *J. Res. Natl. Bur. Stands. A. Physics and Chemistry*. 73A, 5, 1969, 479–485.

[12]. D.F. Williams, "Assessment of candidate molten salt coolants for the NGNP/NHI Heat-Transfer Loop", Oak Ridge National Laboratory, ORNL/TM-2006/69, 2006.

[13] A.C. Victor and T.B. Douglas "Thermodynamic Properties of Magnesium Oxide and Beryllium Oside from 298 to 1200 K" *J. Res. Natl. Bur. Stands. A. Physics and Chemistry*. 67A, 4, 1963, 325–329.

[14] R. A. McDonald, "Heat Content and Heat Capacity of an Extruded Graphite from 341 to 1723 K" *J. Chem. Eng. Data*. 10, 3, 1965, 243.

Appendix A: Material Certificates for Salt Reagents

Figure A.1 Certificate of Analysis for LiF

Specification

1.05686.0050   Lithium fluoride 99.99 Suprapur®

	Specification	
Purity (metallic)	≥ 99.99	%
Ba (Barium)	≤ 5.0	ppm
Ca (Calcium)	≤ 2.0	ppm
Cd (Cadmium)	≤ 0.5	ppm
Co (Cobalt)	≤ 0.5	ppm
Cs (Cesium)	≤ 20	ppm
Cu (Copper)	≤ 0.5	ppm
Fe (Iron)	≤ 0.5	ppm
K (Potassium)	≤ 10	ppm
Mg (Magnesium)	≤ 0.5	ppm
Mn (Manganese)	≤ 0.5	ppm
Na (Sodium)	≤ 10	ppm
Ni (Nickel)	≤ 0.5	ppm
Pb (Lead)	≤ 0.5	ppm
Rb (Rubidium)	≤ 10	ppm
Sr (Strontium)	≤ 5	ppm
Zn (Zinc)	≤ 0.5	ppm

Evelyn Allmann
Responsible laboratory manager quality control

This document has been produced electronically and is valid without a signature.

Figure A.2 Certificate of analysis for NaF.

SIGMA-ALDRICH®

sigma-aldrich.com

3050 Spruce Street, Saint Louis, MO 63103, USA
Website: www.sigmaaldrich.com
Email USA: techserv@sial.com
Outside USA: eurtechserv@sial.com

Certificate of Analysis

Product Name:
Sodium fluoride – anhydrous, powder, 99.99% trace metals basis

Product Number:	450022	
Batch Number:	MKBV9645V	
Brand:	ALDRICH	
CAS Number:	7681-49-4	
MDL Number:	MFCD00003524	
Formula:	FNa	
Formula Weight:	41.99 g/mol	
Quality Release Date:	17 JUL 2015	
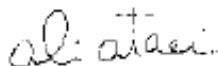
NaF

Test	Specification	Result
Appearance (Color)	White	White
Appearance (Form)	Powder	Powder
Gravimetric Analysis		45.3 %
% F With Lead Acetate		
ICP Major Analysis	Confirmed	Conforms
Confirms Sodium Component		
Purity	Meets Requirements	Meets Requirements
99.99% Based On Trace Metals Analysis		
Trace Metal Analysis	≤ 150.0 ppm	31.3 ppm
Aluminum (Al)		0.6 ppm
Barium (Ba)		0.5 ppm
Calcium (Ca)		1.5 ppm
Cesium (Cs)		5.0 ppm
Iron (Fe)		14.2 ppm
Potassium (K)		6.6 ppm
Lithium (Li)		0.9 ppm
Magnesium (Mg)		1.3 ppm
Manganese (Mn)		0.3 ppm
Rubidium (Rb)		0.4 ppm
Strontium (Sr)		< 0.1 ppm

Ali Atael, Manager

Figure A.3 Certificate of analysis for KF.

Certificate of Analysis

Product Name:
Potassium fluoride – anhydrous, powder, ≥99.9% trace metals basis

Product Number:	449148
Batch Number:	MKBX2566V
Brand:	ALDRICH
CAS Number:	7789-23-3
MDL Number:	MFCD00011398
Formula:	FK
Formula Weight:	58.10 g/mol
Quality Release Date:	31 DEC 2015

KF

Test	Specification	Result
Appearance (Color)	White	White
Appearance (Form)	Powder	Powder
ICP Major Analysis	Confirmed	Confirmed
Confirms K Component		
Purity	Conforms	Conforms
>=99.9% Based On Trace Metals Analysis		
Trace Metal Analysis	$\leq$ 1000.0 ppm	614.7 ppm
Boron (B)		1.4 ppm
Calcium (Ca)		3.0 ppm
Chromium (Cr)		2.1 ppm
Cesium (Cs)		12.7 ppm
Iron (Fe)		8.4 ppm
Lithium (Li)		1.9 ppm
Manganese (Mn)		0.9 ppm
Sodium (Na)		527.4 ppm
Rubidium (Rb)		57.0 ppm

Michael Grady, Manager
Quality Control
Milwaukee, WI US

Figure A.4 Certificate of analysis for BeF$_2$.

MATERION
CERTIFICATE OF ANALYSIS

Customer: University of Chicago Argonne, LLC
Argonne National Laboratory
Building 46
9700 S. Cass Avenue
Lemont, IL 60439-4874
Material Description:

Date: 05/24/2019
Sales Order: 625877
P.O. 9A-64875

Specification: Be Fluoride

Item 10: 5.00 kg Be Fluoride

CHEMICAL COMPOSITION: (%)					MECHANICAL PROPERTIES						
Lot	19-05-01										
Be	19.2										
BeF$_2$	100										
Fe	<.01										
Al	<.02										
Na	.06										
Mn	<.002										
Cr	<.002										
Ni	<.004										

ADDITIONAL INFORMATION:

Materion testing for chemistry composition, mechanical and physical properties were tested at our laboratory in Elmore, OH or as necessary, outside laboratories under control of the Elmore Quality Department.
This material was inspected and tested and is conforming as required in accordance with the noted part, specification, drawing and revision. The test methods for these tests are available for review by the buyer.
This is to certify that during the manufacturing, process, examination, testing and packaging, our products do not come in contact with mercury or any of its compounds nor with any mercury-containing devices employing a single boundary or containment.

MATERION BRUSH INC.
QUALITY CONTROL

QA96-181-0

Chemical and Fuel Cycle Technologies Division

Argonne National Laboratory
9700 South Cass Avenue, Bldg. 205

Lemont, IL 60439

www.anl.gov